

# Synchrotron radiation from quasi-monoenergetic electrons

## Modelling the spectrum of Sgr A\*

T. Beckert<sup>1</sup> and W.J. Duschl<sup>1,2</sup>

<sup>1</sup> Institut für Theoretische Astrophysik der Universität Heidelberg, Tiergartenstr. 15, D-69121 Heidelberg, Germany

<sup>2</sup> Max-Planck-Institut für Radioastronomie, Auf dem Hügel 69, D-53121 Bonn, Germany

Received ...; accepted ...

**Abstract.** We investigate the spectrum of a quasi-monoenergetic ensemble of relativistic electrons, especially for the mildly relativistic case, and discuss the effect of inclination of the magnetic field on the emissivity. We apply the exact theoretical description to the spectrum of the radio source Sgr A\* which is located at or very close to the dynamical center of our Galaxy. We find that the radio-MIR spectrum can be reproduced well, but that the resulting self-comptonized X-ray flux is much smaller than the observed one.

**Key words:** Galaxy: center – Radiation mechanisms: non-thermal – Radio continuum: general – X-rays: general

### 1. Introduction

Observations of the galactic center radio source Sgr A\* in the last few years (e.g. Zylka et al. 1995) have raised the interest in detailed investigations of synchrotron spectra produced by mildly relativistic electrons (e.g. Melia 1994, Mahadevan et al. 1996). [Melia (1994)] proposed synchrotron radiation from thermal electrons in a radial inflow but failed to explain the latest sub-mm data. Narayan et al. (1995) presented a model for the entire spectral range from radio to X-ray frequencies based on advection dominated accretion.

In our view, only the radio observations can be taken as firm detections and the best fit from accretion models with LTE is based on a isothermal sphere emitting optically thin synchrotron radiation. In a previous paper (Beckert et al. 1996, hereafter referred to as B96) we showed that a homogeneous blob of relativistic electrons penetrated by a magnetic field is sufficient to explain the observed spectrum.

In the present paper we describe the calculation of synchrotron spectra of electrons with various distributions in momentum space as seen by an arbitrary observer. The basic equations are presented in Sect. 2 and Appendix A. We apply the general formulae (e.g. [Bekefi 1966]) without approximations to a source of mildly to highly relativistic electrons. In Sect. 3

we discuss in detail the synchrotron spectrum of monoenergetic electrons and compare the results with the standard treatment for highly relativistic electrons. In Sect. 4 we provide a criterion for quasi-monoenergetic distributions and show the deviations from a simple approximation to the synchrotron spectra which is used to identify optically thin monoenergetic synchrotron sources (Duschl & Lesch 1994, Reuter & Lesch 1996). In the subsequent Sect. 5 we derive the synchrotron flux of homogeneous spherical sources with optical thick-thin transition. Sect. 6 deals with the application of quasi-monoenergetic electron distributions to the observations of Sgr A\*. We interpret the low-frequency turn-over (B96) in terms of synchrotron self-absorption (SSA) and determine the physical source parameters under the assumption of energy equipartition between electrons and magnetic field. An unavoidable consequence of the synchrotron model is the self-comptonization of the emitted radiation (SSC) which emerges as X-rays, briefly discussed in Sect. 7. We summarize our results in Sect. 8.

### 2. Synchrotron Theory

The theory of synchrotron emission has been reviewed several times ([Bekefi 1966], Ginzburg & Syrovatsky 1969). Here we briefly discuss the basic formulae for the coefficient of spontaneous emission and for the observed power of synchrotron radiation of single electrons. The fundamental work was done by Schwinger (1949) and Westfold (1959), but later on the difference in observed and emitted power of single electrons was recognized by Epstein & Feldman (1967) and Scheuer (1968). We use a formulation of synchrotron emission based on the retarded potentials to calculate the received power seen by a distant observer. Radiation losses are neglected and we assume that binary encounters do not take place. The relativistic electrons are characterised by their energy  $E = \gamma m_e c^2$ , the orbital frequency

$$\omega_s = \frac{qB}{\gamma m_e c} \quad \gamma = \frac{1}{\sqrt{1 - |\beta|^2}} \quad (1)$$

in a locally homogeneous magnetic field  $B$  and a pitch angle  $\alpha$  between the magnetic field and the momentum of the spiraling electron. The electric and magnetic radiation field which

Send offprint requests to: T. Beckert (tbec@ita.uni-heidelberg.de)

determine the flux density are periodic in the retarded time of emission  $\tau$

$$t = \tau + \frac{R(\tau)}{c} \quad (2)$$

Rather than performing a Fourier transformation to get the spectral emissivity of a single particle in a homogeneous magnetic field we expand the radiation field in a Fourier series. The received power per steradian in a direction  $\theta$  to the magnetic field is derived in Appendix A and reads

$$P = \frac{q^2}{2\pi c} \sum_{m=1}^{\infty} |g_m|^2 \quad (3)$$

with a complex field vector

$$\mathbf{g}_m = \frac{m\omega_s}{\xi^2} \begin{pmatrix} \beta \sin \alpha J'_m(m\psi) \\ i(\beta \cos \alpha - \cos \theta) \sin \theta^{-1} J_m(m\psi) \\ 0 \end{pmatrix} \quad (4)$$

depending on the geometric quantities

$$\psi = \frac{\beta \sin \alpha \sin \theta}{\xi} \quad \xi = 1 - \beta \cos \alpha \cos \theta \quad (5)$$

The coefficient of spontaneous emission  $\eta_\nu$  which is related to the emissivity by  $j_\nu = \int d^3p \xi f(p) \eta_\nu(p)$  is obtained with a resonance condition  $\delta(\nu - m\nu_s \xi^{-1})$ , since we are dealing with emission at discrete frequencies  $\nu = m\nu_s \xi^{-1}$ .

$$\eta_\nu = \frac{q^2 (2\pi\nu)^2 \beta^2}{2\pi c \xi^2} \sum_{m>1} \delta(\nu - m\nu_s \xi^{-1}) \times \left[ (\sin \alpha J'_m(m\psi))^2 + (g_1 J_m(m\psi))^2 \right] \quad (6)$$

$$g_1 = \left( \frac{\beta \cos \alpha_m - \cos \theta}{\beta \sin \theta} \right) \quad (7)$$

This form of the spontaneous emission differs from the standard form (e.g. [Bekefi 1966]) by an additional factor  $\xi^{-1}$ . In the standard calculation a square of  $\delta$ -functions appears. From our point of view, one of these is replaced by  $\omega_s^{-1}$  and divided by  $T = 2\pi\omega_s^{-1}$  to get the mean power from the total energy. But the frequency  $\nu_s = T^{-1}$  is not the observed frequency  $\nu = \xi\nu_s$  of the radiation. This additional  $\xi$  is contained in our Eq. (6). We will in see Sec. 3 that this difference is offset by the normalization of the distribution function in calculating the spectral emissivity.

### 3. Synchrotron spectra of monoenergetic electrons

We describe the radiating electrons by a stationary distribution function  $f_e(\alpha, p)$  in momentum space in a homogeneous magnetic field. The distribution in phase space is assumed to be separable and the complete distribution function looks like  $n(\mathbf{r})f_e(\alpha, p)$  with the volume density  $n(\mathbf{r})$ . In order to recover the standard description of emissivity we must consider the distribution  $f_e$  in the observers frame. We take  $f_e$  to be normalized so that the density of electrons in the source is contained in  $n(\mathbf{r})$ . In principle, the distribution is a density and can be time dependent. While the distribution describes the electrons in the source at time  $\tau$ , we have changed the time variable to

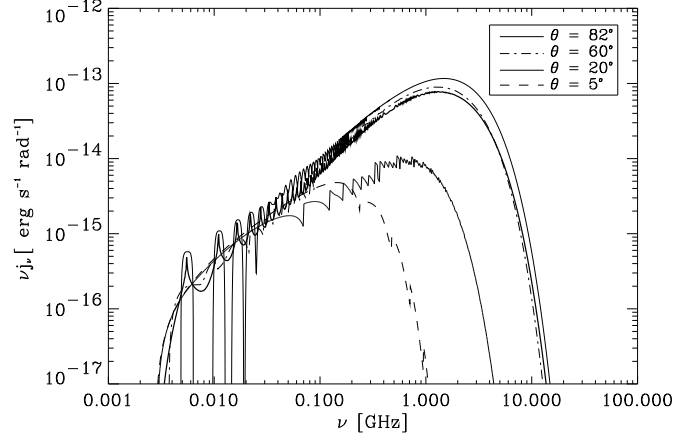


**Fig. 1.** The spectrum of mildly relativistic electrons with  $\gamma = 5$  seen by observers at  $\theta = 5^\circ, 20^\circ, 60^\circ, 82^\circ$ . We plot the received power  $\nu j_\nu$  for a normalized distribution. The spectra obtain their maxima at higher frequencies as observers approach  $\theta = 90^\circ$ . The thickest solid line is the average of all observers corresponding to an isotropic distribution of magnetic field directions.

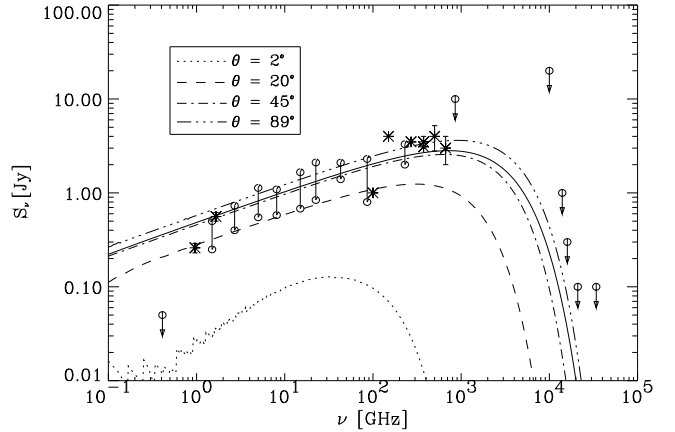


**Fig. 2.** The flux density distribution of Sgr A\* fitted with monoenergetic electrons of 140 MeV corresponding to  $\gamma = 275$ . The observed spectrum is taken from B96 where symbols with circles at both ends indicate variability. The solid curve corresponds to the mean observer position and broken lines refer to  $\theta = 89^\circ, 45^\circ, 20^\circ, 2^\circ$  from high to low flux densities at 10 GHz. For physical parameters, see model I in Tab.1.

the time of observation  $t$ . This transformation is reflected in the differential  $dt = \xi d\tau$  and the distribution seen by the observer is therefore  $\xi f_e(\alpha, p)$ . A more extended discussion of this argument is given in Appendix B. The integrated spectral emissivity in the observers frame follows from the power of a single electron stated above

$$j = \frac{q^2}{c} \int_0^\infty dp p^2 \int_0^\pi d\alpha \sin \alpha \xi f_e(\alpha, p) \sum_{m=1}^{\infty} |g_m|^2 \quad (8)$$

The spectral emissivity is obtained from the spontaneous emission given in Eq. (6) by evaluating the  $\alpha$ -integration. The  $\delta$ -function fixes  $\alpha$  for each combination of  $[\nu, \theta \neq \frac{\pi}{2}, m]$  unambiguously by

$$\cos \alpha_m = \frac{1 - \frac{m\nu_s}{\nu}}{\beta \cos \theta} \quad (9)$$

Since  $\alpha_m \in [0, \pi]$  has to be a real number, we get a condition for the index  $m$

$$\frac{\nu}{\nu_s}(1 - \beta|\cos \theta|) \leq m \leq \frac{\nu}{\nu_s}(1 + \beta|\cos \theta|) \quad (10)$$

It turns out that the problem of deducing the spectrum of a distribution of electrons in momentum space is reduced to one integral and a limited sum of Fourier coefficients :

$$j_\nu(\Omega) = n(r) \frac{4\pi^2 q^2 \nu}{c} \int_0^\infty dp p^2 \sum_m \frac{\beta f_e(\alpha_m, p)}{|\cos \theta|} \times \left[ (\sin \alpha_m J'_m(m\psi))^2 + (g_1 J_m(m\psi))^2 \right] \quad (11)$$

The abbreviation  $g_1$  appeared previously in Eq. (7). This form is an exact result with  $\alpha_m$  determined by Eq. (9). The sum can be evaluated directly for small frequencies  $\nu \sim \nu_s$  and small momenta where only a few cyclotron lines emerge in the spectrum. For frequencies where the range of indices  $m$  for the harmonics contributing to the sum is wide, it is reasonable to transform the sum to an integral and evaluate it numerically.

For a monoenergetic and isotropic distribution, the distribution function is  $f_e(\alpha_m, p) = (4\pi p_0^2)^{-1} \delta(p - p_0)$  and the emissivity in Eq. (11) consists of contributions from electrons described by  $(\alpha_m, p_0)$  whose  $m$ -th harmonic is shifted to the frequency  $\nu$  in the direction of the observer. The resulting spectrum is shown for four different observers in Fig. 1, for electrons with a common Lorentz factor of  $\gamma = 5$  corresponding to 2.56 MeV. We see that the average of all observers is similar to the emission in the direction  $\theta = 60^\circ$  shown by the dashed line in the Figure. The received flux changes drastically when the direction to the observer becomes parallel to the magnetic field lines. The emission for  $\theta = 5^\circ$  consists of overlapping low  $m$ -harmonics of electrons with small pitch angles. In addition, it demonstrates the transition from overlapping cyclotron lines to a continuous synchrotron spectrum. The flux measured by the observer is increased relative to the emitted power of the spiraling electron which mainly radiates in the direction parallel to its momentum. Ginzburg et al. (1968) recognized that there also is a change in the total energy of the radiation field inside a fixed sphere in the observers frame containing the electron and the observer at its surface.

The synchrotron spectra of monoenergetic electrons provide a reasonable fit to the Sgr A\* spectrum except for the turn-over below 1 Ghz. We have taken the average of all observer positions and a magnetic field strength of 10 G, comparable to the first model using monoenergetic electrons by Duschl & Lesch (1994). The  $\theta$ -dependency is increased for high energies as seen in Fig. 2. The parameters are combined in Tab. 1 as model I and discussed in greater detail in Sect. 6.

So far we have a description for the spontaneous emission. To get a complete spectrum, we must include induced emission

and absorption inside the source. The cross section for synchrotron self-absorption (SSA) is basically given by

$$\sigma_\nu = \frac{c^2}{8\pi h \nu^3} \int_0^\infty dp p^2 (f(p_1) - f(p)) \epsilon_\nu(p) \quad (12)$$

where  $p_1$  is the momentum of the electron before absorption. The relativistic limit - which we assume for SSA - is simply  $p_1 c = pc - h\nu$ . The emissivity  $\epsilon_\nu(p)$  is the  $\theta$ -average of  $j_\nu$  per electron. In principle the emissivity has to be split up into the two directions of polarisation present in Eq. (4) and the cross-section must be calculated separately for both directions. Since we assume that the distribution of magnetic field directions is isotropic on a length scale much shorter than the source size, this distinction can be omitted without introducing relevant errors. Using a Taylor-expansion for  $f(p_1) - f(p)$  we get an expression which closely resembles the standard formula and can easily be evaluated numerically.

$$\sigma_\nu = \frac{c^2}{8\pi h \nu^3} \int_0^\infty dp (p_1 - p) \frac{\partial}{\partial p} f \sum_m \frac{\beta \nu}{m \nu_s |\cos \theta|} |g_m|^2 \quad (13)$$

All low frequency turn-overs seen in the spectra of Fig. 6 - 10 are due to synchrotron self-absorption.

#### 4. A criterion for quasi-monoenergetic distributions

Until now we have not defined what we call a quasi-monoenergetic electron distribution. To do this we compare the exact formulae given in Sec. 3 with a simple approximation for the emissivity of monoenergetic electrons in the energy range  $\gamma = 100 \dots 1000$ . This will allow us to derive analytic expressions for the emissivity of truncated power-law distributions. From these we get a criterion what a quasi-monoenergetic distribution will be when synchrotron emission is considered. We approximate the synchrotron spectrum of a single electron by

$$P(\nu, \gamma) = P_0 \nu^{1/3} \exp[-\nu/\nu_c] \quad (14)$$

which is used in the interpretation of the radio spectra of Sgr A\* (Duschl & Lesch 1994) and the core of M81 (NGC3031) by Reuter & Lesch (1996). The total luminosity of a single electron is

$$L = L_0 B^2 (\gamma \beta \sin \alpha)^2$$

with pitch angle  $\alpha$  in the frame of the source and

$$L_0 = 1.5870 \cdot 10^{-15} \text{erg s}^{-1}$$

if the magnetic field is measured in Gauss. In the observers frame the shift of time intervals  $dt = \xi d\tau$  introduces a factor  $\xi^{-1}$  as discussed in Sec. 3 and in Appendix B. For sufficiently high electron energies and frequencies much larger than the orbital frequency, the radiation is beamed in the direction  $\alpha \approx \theta$  and we approximate  $\xi \approx \sin^2 \alpha$ . The observed luminosity becomes independent of the pitch angle :

$$L = L_0 B^2 \gamma^2$$

The scaling of the spectral power  $P(\nu, \gamma)$  is obtained from the luminosity and gives

$$\nu_c = \nu_0 \gamma^2 = \frac{\kappa B q \gamma^2}{2\pi m c} \quad (15)$$

$$P_0 = \frac{3}{\Gamma(1/3)} L_0 B^{2/3} \gamma^{-2/3} \left( \frac{2\pi mc}{\kappa q} \right)^{4/3}$$

As a factor in the critical frequency  $\nu_c$  we introduced a coefficient  $\kappa$  which is usually taken as  $\kappa = 1.5$ . We would like to compare the approximation with the exactly evaluated spectra and minimize the relative error. This suggests a smaller value for  $\kappa \approx 1.2$  so that the error is less than 20% in the range  $100 < \gamma < 1000$  as shown in Fig. 3. We restrict the error box in Fig. 3 to frequencies around the maximum of the flux. At high frequencies  $\nu > 5\nu_c$  the spectrum drops nearly exponentially and the flux has decreased by two orders of magnitude. At low frequencies the spectrum is changed by the presence of cyclotron lines which provide a significantly smaller flux. But the absolute flux is small at low frequencies due to the approximated  $P_\nu \sim \nu^{1/3}$  behavior and is often suppressed by self-absorption. In order to get analytic expressions which

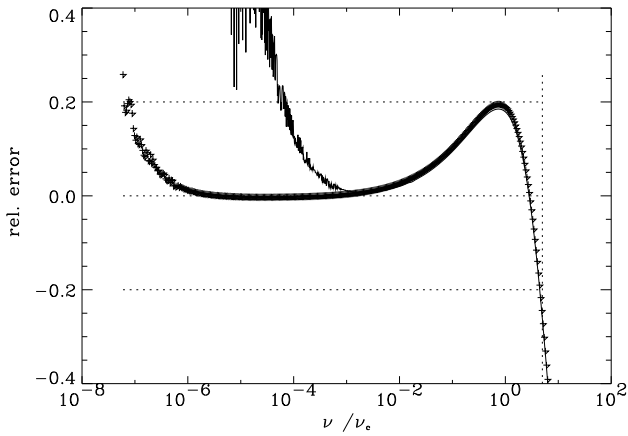


**Fig. 3.** Relative error of the simple approximation Eq.(14) compared with the monoenergetic case averaged over the observer positions  $\theta$ . The crosses indicate the error for  $\gamma = 1000$  and the solid line for  $\gamma = 100$ . The deviations at small frequencies are dominated by the discrete cyclotron lines present in the strict monoenergetic case. The magnetic field is taken as  $B = 10$  G.

determine what we want to call a quasi-monoenergetic electron distribution, we investigate restricted power-laws  $f_0 \gamma^{-\alpha}$  for  $\gamma_1 < \gamma < \gamma_2$  and set the distribution to zero for other energies. The width  $\chi$  of the distribution is defined as  $\chi = \gamma_2/\gamma_1$  and is the main parameter in our investigation. The mean luminosity is then

$$\langle L \rangle = n(r) L_0 B^2 \langle \gamma \rangle^2 \frac{Q^2(2)}{Q(1)Q(3)}$$

$$Q(x) = \left( \frac{x - \alpha}{\chi^{x-\alpha} - 1} \right)$$

We normalize the distribution function so that  $n(r)$  gives the spatial density of the relativistic electrons.

$$n(r, \gamma) = n(r) f_0 \gamma^{-\alpha}$$

$$f_0 = \gamma_1^{\alpha-1} Q(1) \quad \langle \gamma \rangle = \gamma_1 \frac{Q(1)}{Q(2)}$$

We assume equipartition between magnetic and kinetic energy density. Despite the presence of a thermal plasma, we only consider the relativistic electrons in the kinetic energy. The spatial density

$$n(r) = \frac{B^2}{8\pi mc^2} \langle \gamma \rangle^{-1}$$

is thus unambiguously determined by the magnetic field and the mean electron energy. In the discussion of quasi-monoenergetic distributions, we want to redefine the critical frequency given in Eq.(15) by replacing the square of the relativistic  $\gamma$ -factor by the square of the mean  $\langle \gamma \rangle^2$

$$\nu_c = \frac{\kappa B q \langle \gamma \rangle^2}{2\pi mc}$$

The mean emissivity is

$$j_\nu = j_0 B^{8/3} \nu^{1/3} \langle \gamma \rangle^{-5/3} G \quad (16)$$

with

$$j_0 = \frac{3L_0}{32\pi^2 \Gamma(1/3) mc^2} \left( \frac{2\pi mc}{\kappa q} \right)^{4/3}$$

$$G = \gamma_1^{\alpha-1/3} Q^{5/3}(1) Q^{-2/3}(2) U \quad (17)$$

$$U = \int_{\gamma_1}^{\gamma_2} d\gamma \gamma^{-\alpha-2/3} \exp[-\nu/\nu_0/\gamma^2]$$

If  $\nu \ll \nu_c$  we find  $G \approx Q^{5/3}(1) Q^{-2/3}(2) Q^{-1}(1/3)$ . To see the effect in the frequency range  $\nu \approx \langle \gamma \rangle^2 \nu_0$  we must evaluate the correct integral  $U$ . We introduce a new variable  $s = \nu \nu_0^{-1} \gamma^{-2}$  and find :

$$U = \left( \frac{\nu_0}{\nu} \right)^{\frac{\alpha}{2} - \frac{1}{6}} \int_{s_2}^{s_1} ds s^{\alpha/2 - 7/6} \exp[-s]$$

$$\nu_0 = \frac{3Bq}{4\pi mc}$$

The integral  $U$  can be expressed as the difference of two incomplete Gamma-functions  $\gamma(a, x)$

$$U = \left( \frac{\nu_0}{\nu} \right)^{\frac{\alpha}{2} - \frac{1}{6}} \left( \gamma \left( \frac{\alpha}{2} - \frac{1}{6}, \frac{\nu}{\nu_0 \gamma_1^2} \right) - \gamma \left( \frac{\alpha}{2} - \frac{1}{6}, \frac{\nu}{\nu_0 \gamma_2^2} \right) \right)$$

or as the difference between two confluent hypergeometric functions  $M(a, b, z)$  (Kummer functions) resulting in a compact form for  $G$

$$G = 2e^{-\frac{\nu}{\nu_c}} Q^{5/3}(1) Q^{-2/3}(2) \left( \frac{\chi^{1/3-\alpha} \hat{Q}(\gamma_2) - \hat{Q}(\gamma_1)}{\frac{1}{3} - \alpha} \right)$$

$$\hat{Q}(\gamma) = \exp \left[ -\nu/\nu_0 \left( \gamma^{-2} - \langle \gamma \rangle^{-2} \right) \right] M \left( 1, \frac{\alpha}{2} + \frac{5}{6}, \frac{\nu}{\nu_0 \gamma^2} \right)$$

The changes in the synchrotron spectra become significant when the width of the distribution grows beyond a limit of say  $\chi = 5$ . In that case the effect of the broader distribution exceeds the error introduced in the approximation Eq. (14). The effect of the width on the approximate spectra are shown in Fig. 5 where the solid line corresponds to  $\chi = 7$ .

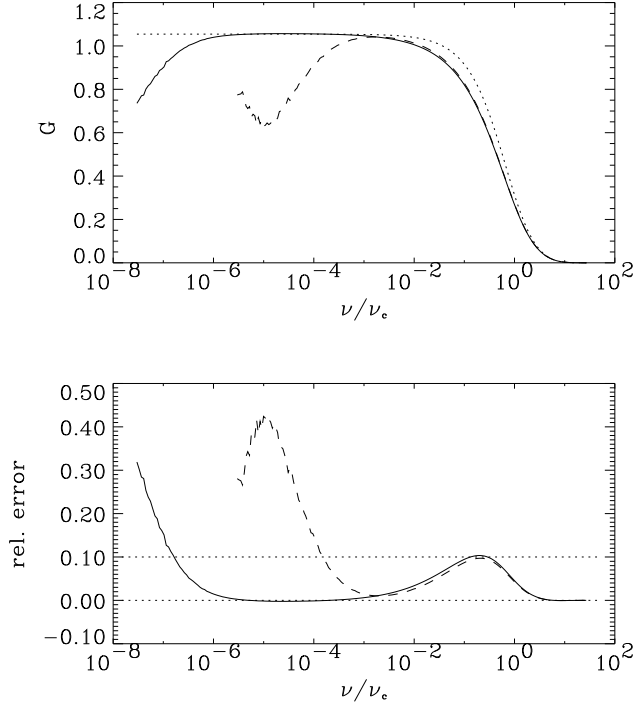


**Fig. 4.** Comparison of the approximation Eq. (17) to the numerical evaluation of Eq. (11) for a truncated power-law of width  $\chi = 3$ ,  $\alpha = 2$  averaged over all observers. The approximation is shown as a dotted line and the numerical equivalents are plotted for  $B = 10$  G and  $\gamma = 1000$  (solid) and  $\gamma = 100$  (dashed). The lower panel presents the relative error of the approximation. The dotted lines mark the 0% and 10% level.

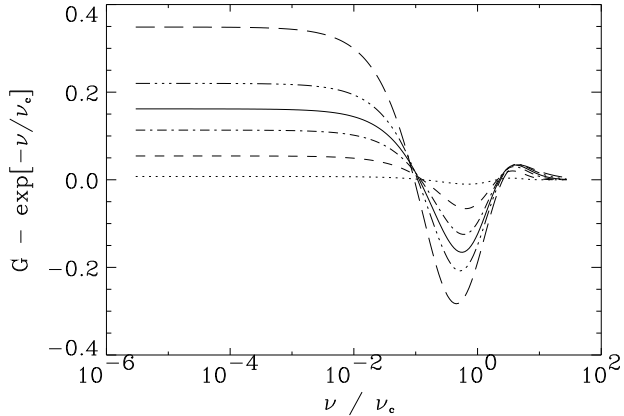


**Fig. 5.** Deviations of the synchrotron spectra of quasi-monoenergetic electrons from the strictly monoenergetic case. We took power-laws with  $\alpha = 2$  and plot  $G - \exp[-\nu/\nu_c]$  as defined in Eq. (17). The deviations grow with  $\chi = 1.5, 3, 5, 7, 10, 20$ .

For a homogeneous, spherical, optically thin source of radius  $R$  we find for the received flux at a distance  $d$

$$S_\nu = 2.01 \cdot 10^{-20} \left[ \frac{R}{1\text{AU}} \right]^3 \left[ \frac{d}{1\text{kpc}} \right]^{-2} \left[ \frac{B}{1\text{G}} \right]^{\frac{8}{3}} \left[ \frac{\nu}{1\text{GHz}} \right]^{\frac{1}{3}} \times \langle \gamma \rangle^{-\frac{5}{3}} G \text{ erg s}^{-1} \text{ Hz}^{-1} \text{ cm}^{-2} \quad (18)$$

with the coefficient  $\kappa$  taken to be 1.2. For completeness we present the absorption coefficient for synchrotron self-absorption in the same approximation as above for the emissivity. Inserting the mean emissivity from Eq. (16) in Eq. (12) we get

$$\alpha_\nu = \alpha_0 B^{\frac{8}{3}} \nu^{-\frac{5}{3}} \langle \gamma \rangle^{-\frac{8}{3}} Q^{8/3}(1) Q^{-5/3}(2) J$$

$$\alpha_0 = \frac{c^2 j_0}{2} = \frac{3L_0}{(8\pi)^2 \Gamma(\frac{1}{3}) m} \left( \frac{4\pi mc}{3q} \right)^{4/3}$$

$$J = (2 + \alpha) \gamma_1^{\alpha+2/3} \tilde{J}$$

$$\tilde{J} = \int_{\gamma_1}^{\gamma_2} d\gamma \gamma^{-\alpha-5/3} \exp \left[ -\frac{\nu}{\nu_0 \gamma^2} \right]$$

We will not discuss synchrotron self-absorption further in this approximation.

## 5. Aspects of radiative transfer in a homogeneous and spherical source

We assume that the strength of the magnetic field  $B$ , the density of relativistic electrons  $n(r)$  and the energy distribution of the electrons are constant throughout the source. As a consequence, the emissivity  $\epsilon_\nu$  and the absorption coefficient  $\alpha_\nu$  do not depend on the location inside the source. This simplifies the radiative transfer so that we can get analytic expressions for the synchrotron flux at the surface. At first we find for the intensity

$$I_\nu = \frac{j_0}{\alpha_0} \nu^2 \frac{Q(2) \langle \gamma \rangle}{(2 + \alpha) Q(1) \gamma_1 \tilde{J}} \frac{U}{\tilde{J}} (1 - \exp[-\alpha_\nu s])$$

if  $s$  is the length of the path through the blob. Here we have again assumed energy equipartition as in Sec. 4. If we integrate over the surface in the sky we find a total flux

$$F_\nu = 2\pi \frac{\nu^2}{c^2} \frac{Q(2) \langle \gamma \rangle}{(2 + \alpha) Q(1) \gamma_1 \tilde{J}} \times \left( R^2 + \frac{R}{\alpha_\nu} e^{-2\alpha_\nu R} - \frac{e^{-\alpha_\nu R}}{\alpha_\nu^2} \sinh(\alpha_\nu R) \right) \quad (19)$$

In the optically thick regime the flux is proportional to the area  $2\pi R^2$  and in the optically thin case we perform a Taylor expansion and recover the simple form

$$F_\nu \approx \frac{4\pi}{3} R^3 j_\nu \left( 1 - \frac{3}{4} R \alpha_\nu \right)$$

to first order in in the optical depth  $R\alpha_\nu$ .

**Table 1.** Physical parameters for the synchrotron source Sgr A\*

Model	$\langle E[\text{MeV}] \rangle$	$B[\text{G}]$	$R[10^{13} \text{ cm}]$	$n[10^3 \text{ cm}^{-3}]$
I	140	10	1.25	18.0
II	217	2.7	4.92	0.84
III	222	3.0	4.86	1.01
IV	210	4.0	3.75	1.90
V	202	4.0	3.50	1.97

## 6. Application to the galactic center source Sgr A\*

The idea of monoenergetic relativistic electrons producing optically thin synchrotron radiation has been applied to Sgr A\* by Duschl & Lesch (1994). Later on, Narayan, Yi & Mahadevan (1995) showed that thermal electrons in an advection dominated accretion flow can lead to quite similar spectra, but an isothermal sphere seems to fit the data better. In B96 we discussed power-laws for isotropic electron distributions of limited width with infinitely steep cut-offs and emphasized the importance of the absorption mechanism for determining the source parameters. Here, we extend the distributions from the strict monoenergetic case discussed above to include more realistic power-laws with different cut-offs and relativistic thermal distributions. The spectra in B96 were derived for a position angle of  $\theta = 60^\circ$  and in Sect. 3 we showed that this is a good approximation to the average of all possible position angles. Here we always take the average of all directions of magnetic field lines. For a complete description of the source, we assume energy equipartition in order to relate the magnetic field strength with the number density of electrons. We calculate the spectral flux density according to Eq. (19) and adopt a distance of 8.5 kpc to Sgr A\*. The model v in Tab. 1 is the best fit with a truncated power-law distribution as discussed in Sec. 4 and B96.

### 6.1. Power-laws with exponential cut-offs

In B96 we introduced infinitely steep cut-offs for power-law distributions to achieve an easier understanding of the characteristics of synchrotron emission from quasi-monoenergetic electron distributions. They are not expected from acceleration mechanisms for electrons in a relativistic plasma. However, distribution functions with an exponential cut-off at high energies and a rising power-law at low energies are expected for equilibrium states (e.g. Schlickeiser 1984). If we think of an injection mechanism at high energies like magnetic reconnection, we assume exponential decays at both ends of the distribution and a power-law in between. The distribution, normalized for a single electron, becomes

$$f(p) = K^{-1} p^\sigma \exp \left[ -\frac{p}{p_2} - \frac{p_1}{p} \right] \quad (20)$$

$$K = 2(p_1 p_2)^{\frac{1+\sigma}{2}} K_{1+\sigma} \left( 2\sqrt{\frac{p_1}{p_2}} \right) .$$

The normalization is expressed in terms of modified Bessel functions  $K_z(x)$  of order  $z$ . In contrast with power-laws covering a wide range of electron energies, the spectral power  $\sigma$

does not determine the emission spectrum and is assumed to be  $\sigma = -1$  in our case. The width  $\chi = p_2/p_1$  is defined in the same manner as in Sec. 4. The best possible model obtained with a single homogeneous blob of such electrons is shown in Fig. 6. The physical parameters are given as model II in Tab. 1. In contrast to the spectra with infinitely steep cut-offs, this model cannot account for the measured flux densities in the range 200–1000GHz. The power  $\sigma$  and the width (here  $\chi = 3$ ) are unimportant for this part of the spectrum. It is dominated by an exponential tail beyond  $p_2$ .

### 6.2. Thermal distributions

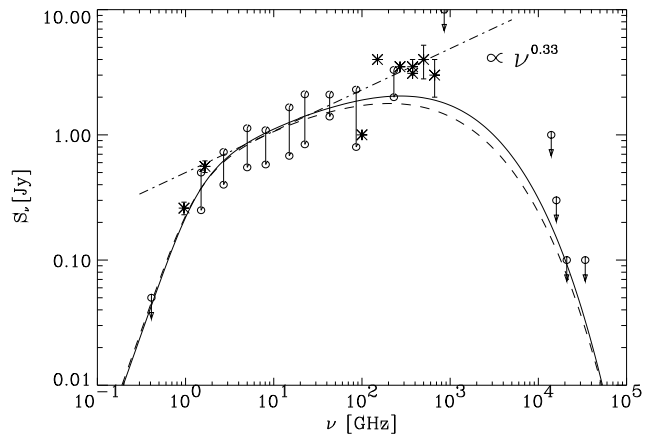


**Fig. 6.** Synchrotron spectrum of electron distributions with exponential high energy tails. Both thermal electrons of  $T = 6 \cdot 10^{11} \text{ K}$  (solid line ; model III in Tab.1) and power-laws with exponential cutoffs (dashed line; model II) at high and low energies can hardly be distinguished.

Another closely related spectrum is produced by relativistic thermal electrons described by a distribution function

$$f(p) = K p^2 \exp \left[ -\frac{\gamma}{\theta_e} \right] ,$$

as seen in Mahadevan et al. (1996) with the corresponding normalisation  $K$  to the number of electrons. The synchrotron spectrum beyond the maxima at  $1.2\gamma^3\nu_s$  is dominated by the exponential decay in the high energy band of the electron spectrum. This is also the case for the distributions with exponential cut-offs discussed above. Obviously, both spatially homogeneous models suffer from the same disease, since they can not explain the sub-mm data seen in Fig.6. The parameters for the thermal distribution are listed as model III in Tab. 1.

### 6.3. A Gauss-Profile for the electron momenta

In the previous example we saw that an exponential high energy tail of the distribution is in contradiction to the assumption

of one single homogeneous blob of optically thin synchrotron emission. A steeper tail is present in a Gaussian profile

$$f(p) = K^{-1} p^2 \exp \left[ -\frac{(p - p_1)^2}{p_2^2} \right] \quad (21)$$

with

$$K = \frac{p_2}{2} \sqrt{\pi} (2p_1^2 + p_2^2)$$

for the norm of the distribution. We have included a phase space

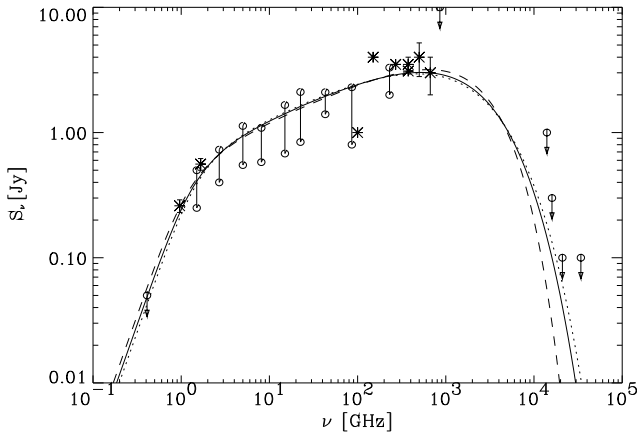


**Fig. 7.** Synchrotron flux from electrons with a gaussian profil in momenta according to model IV in Tab. 1. The width is varied in the range  $\chi = 0.2$  (dashed), 1.0 (solid), 1.92 (dotted) and produce spectra with increasing flux densities at  $2 \cdot 10^4$  GHz.

factor of  $p^2$  which does not affect the resulting spectra very much. Again, the high energy tail is the most important part necessary to explain the sub-mm measurements and yet stay below the upper limits in the IR. We define the width of the Gaussian distribution  $\chi$  as the FWHM  $\Delta p$  of the pure gauss-profile relative to the mean momentum  $p_1$  so that  $\chi = \Delta p/p_1$ . The momentum  $p_2$  is now determined by the width  $p_2 = 0.6 \chi p_1$ . Values greater than 2 are not reasonable for this definition of the width. The obtained fit corresponds to model IV of Tab.1. We see in Fig. 7 that this distribution is sufficient to explain the radio spectrum of Sgr A\* for a wide range of widths up to  $\chi = 1.92$ .

#### 6.4. A core-shell model for Sgr A\*

Since distributions with an exponential high energy tail fail to explain the full spectrum, using the assumption of isotropy and homogeneity of the source, we can build up a two component source. There is good observational evidence for the existence of a central black hole of mass  $M \approx 2.5 \cdot 10^6 M_\odot$  in the galactic center (Eckart & Genzel 1996) which powers Sgr A\*. Accretion into this object implies a special radial structure suggested by Narayan, Yi & Mahadevan (1995). Our first step towards a radial structure is a core-shell model.

**Table 2.** Two component model for the Synchrotron source Sgr A\*

Comp.	$\langle E[\text{MeV}] \rangle$	$B [\text{G}]$	$R [10^{13} \text{ cm}]$	$n [10^4 \text{ cm}^{-3}]$
I	155	2.0	5.5	0.064
II	41.4	70	0.13	300

While the observational situation is far from clear yet, almost simultaneous observations of the spectrum of Sgr A\* from cm to submm wavelengths (Falcke et al. 1997) seem to indicate the possibility of some excess submm flux in comparison to the flux predicted by the homogeneous model.

Our core-shell model consists of an optically thin extended source and a highly self-absorbed compact component. This is not the result of a hydrodynamical calculation, but the best description to explain the observations. The extended part,

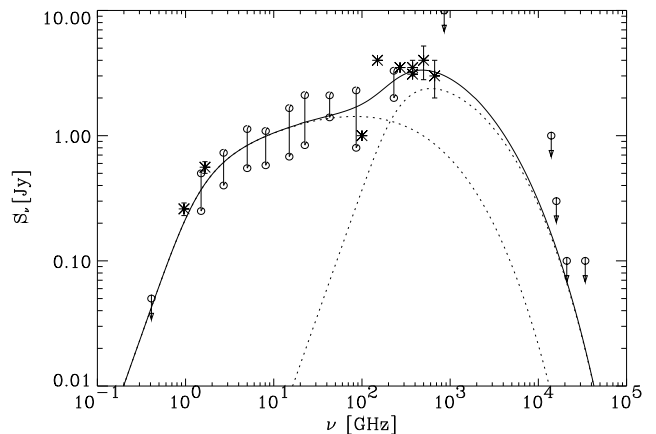


**Fig. 8.** The spectrum of a core-shell model of Sgr A\* consisting of two thermal emitting regions which are homogeneous in itself. The model parameters are given in Tab.2 for the extended shell as part I and the self-absorbed compact core II. Both components are drawn separately as dotted lines.

component I, dominates the spectrum up to 100GHz and has its maximum at lower frequencies compared with the one-component models. The compact component II provides the sub-mm fluxes. This picture is well distinguished from the radial non-uniform self-absorbed source discussed by de Bruyn (1976) which is optically thick at any wavelength, while our model is optically thin between 4 – 100 GHz. The drop of the electron energy inside the compact core is an essential property of the model and is accompanied by a significantly increased magnetic field in the core. The physical parameters are given in Tab. 2.

## 7. Inverse-Compton Spectrum

The first consequence of the interpretation of the radiospectrum as optically thin synchrotron radiation from relativistic elec-

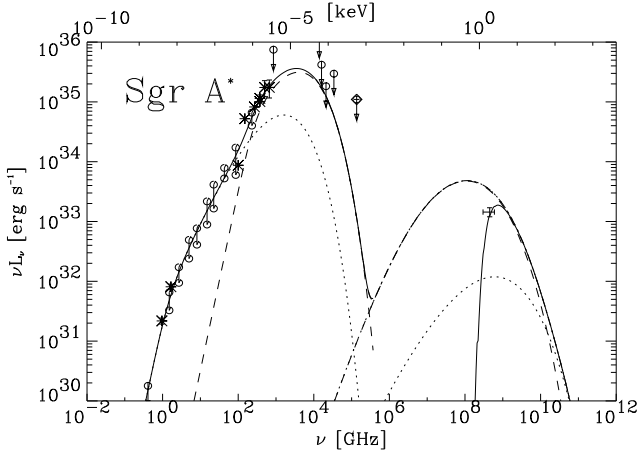


**Fig. 9.** The luminosity of Sgr A\* from the radio to the soft X-ray regime for an assumed distance of 8.5 kpc. The ROSAT flux at 1.85 keV is included. The two-component synchrotron spectrum from a hot ( $T = 6.0 \cdot 10^{11}$  K) extended envelope I and a cooler ( $T = 1.6 \cdot 10^{11}$  K) compact core II (the same as in Fig. 8) is fitted as a solid line. It includes SSC and absorption as discussed in Sec. 7. The intrinsic spectrum of the core (envelope) corresponds to the dashed (dotted) line. The physical parameters are given in Tab.2.

trons is the synchrotron self-comptonization (SSC) process. In this process, only synchrotron photons are considered as the low energy radiation scattered by relativistic electrons. The electron energy distribution  $n_e(\gamma)$  is also obtained from the radiospectrum. From arguments on total cross sections for inverse Compton scattering (Blumenthal & Gould 1970), we can estimate the emitted power due to comptonized synchrotron photons to be

$$P_{\text{Comp}} = \frac{U_{\text{Ph}}}{U_B} P_{\text{Sync}} \quad ,$$

since synchrotron radiation can be considered as Compton scattering of the virtual photons of the static magnetic field. The emitted power is scaled by the relative energy densities of the photon field and the static magnetic field. Taking an intrinsic synchrotron luminosity of  $465 L_{\odot}$  for a gaussian electron distribution and a source radius of  $3.75 \cdot 10^{13}$  cm, we obtain an energy density of  $U_{\text{Ph}} = 3.4 \cdot 10^{-3}$  erg cm $^{-3}$ , which falls short of the energy density of the magnetic field by more than two orders of magnitude. Thus we get a Inverse-Compton luminosity of

$$P_{\text{Comp}} = 4.1 \cdot 10^{33} \left[ \frac{4.0 \text{G}}{B} \right]^2 \left[ \frac{3.75 \cdot 10^{13} \text{cm}}{R} \right]^{-2} \text{ erg sec}^{-1} \quad .$$

The spectrum of the scattered photons can be calculated using the Thomson cross section  $\sigma_T$ , since the synchrotron photons are soft in the electron rest-frame  $\gamma h\nu \ll m_e c^2$ . For an isotropic electron and synchrotron-photon distribution (at least on average), the inverse-Compton flux is

$$F_{\nu} = \frac{3}{16\pi} \sigma_T c h\nu \int d\gamma n_e(\gamma) \int d\nu_s n_s(\nu_s) f(x) \quad (22)$$

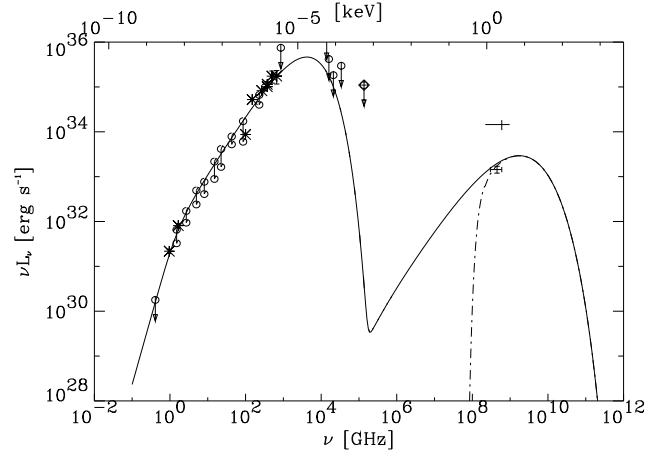


**Fig. 10.** The luminosity of Sgr A\* for assumed distance of 8.5 kpc from the radio to the soft X-ray regime. The model spectrum accounts for synchrotron and single inverse-compton emission. The ROSAT and *Einstein* flux is included. The dashed line is the spectrum including absorption (see text).

where we have used the distribution  $f(x)$  (e.g Blumenthal & Gould 1970) for single scattering events, defined as

$$f(x) = 2x \ln(x) + x + 1 - 2x^2 \quad x = \frac{\nu}{4\nu_s \gamma^2}$$

and the index  $s$  refers to the synchrotron photon distribution and frequency. The mean density of incident photons in a homogeneous spherical source of radius  $R$  with  $\tau = \tau(R) = \alpha_{\nu} R$  and the source function  $S_{\nu_s}$  is given by

$$n_s(\nu_s) = \frac{4\pi}{ch\nu_s} S_{\nu_s} \left( 1 - \frac{1}{\tau} + \frac{1 - e^{-2\tau}}{2\tau^2} \right) \quad .$$

For most distributions, the integrals in Eq. (22) can not be evaluated analytically. The calculated spectrum shown in Fig. 10 is produced by a gaussian electron distribution according to model IV of Tab.1 . The measured flux density in the 0.8 – 2.5 keV range reported by Predehl & Trümper (1994) for ROSAT-PSPC without correction for absorption is included in Fig. 10. We take the upper limit for the ionized hydrogen column density towards Sgr A\* (B96)  $N_{\text{H}} = 2.2 \cdot 10^{21}$  cm $^{-2}$  and obtain a cut-off due to photoelectric absorption (Morrison & McCammon 1983) at approximately 1 keV. SSC and external absorption with the predicted column density from the turn-over at 1 GHz can account for the ROSAT measurement. Other measurements with *Einstein* (Watson et al. 1981) and ART-P (Pavlinisky et al. 1994) are not consistent with this interpretation. The assumed  $N_{\text{H}}$  column density is much too low to account for the visual extinction of approximately 30<sup>mag</sup> corresponding to a canonical hydrogen column density of  $N_{\text{H}} = 6 \cdot 10^{21}$  cm $^{-2}$  towards the galactic center.

## 8. Summary

Synchrotron radiation by quasi-monoenergetic electrons is considered as an explanation of the radio spectrum of the galactic center source Sgr A\*. Therefore, we developed a detailed



treatment of the emission process of single electrons in a homogeneous magnetic field to obtain a correct synchrotron spectrum even for mildly relativistic electron energies. We showed that the emissivity of a single electron is modified due to the relativistic motion of the electrons with respect to the observer compared with the standard theory. This effect is removed when a stationary and isotropic distribution is considered as shown in Appendix B. The spectra of monoenergetic electrons are integrated for various electron distributions covering a thin shell in momentum space. These quasi-monoenergetic electrons in a homogeneous and isotropic source provide a fairly good fit to the time averaged radiospectrum of Sgr A\*. The resulting self-comptonized X-rays are sufficient to explain the ROSAT-observations with a very low hydrogen column density. This hydrogen column density is consistent with the upper limit of ionized hydrogen in the vicinity of Sgr A\* (B96) inferred from free-free absorption. Additional material is required to account for the visual extinction. This may also lead to enhanced absorption in the soft X-ray range and the synchrotron self-comptonization would not be sufficient to explain the flux measured by ROSAT.

Inverted radiospectra showing a synchrotron flux proportional to  $\nu^{0.3}$  are also reported for the centers of M81 (Reuter & Lesch 1996), NGC 1068 (Wittkowski et al. 1997) the archetypal Seyfert 2 galaxy and M 104 (Jauch & Duschl, in preparation). The spectra of all these sources can be interpreted as due to optically thin synchrotron radiation from quasi-monoenergetic electrons. This suggest a new common feature for the centers of normal and active galaxies. The differences in the radio regime arise from the attainable electron energies and the source size.

*Acknowledgements.* We thank the referee, R. Narayan, and R. Mahadevan for helpful remarks which improved the paper, P.G. Mezger for interesting discussions of the subject, and R. Auer for carefully reading the manuscript. This work was supported by the *Deutsche Forschungsgemeinschaft* through SFB 328.

## Appendix A: The Radiation Field at the Observer

The electric field at the position of the observer can be expressed in terms of source properties at the retarded time (Jackson 1962)

$$\mathbf{E} = \frac{q}{cR} \mathbf{g} \quad (\text{A1})$$

$$\mathbf{g}(t) = \frac{\mathbf{n} \times (\mathbf{n} - \boldsymbol{\beta}) \times \dot{\boldsymbol{\beta}}}{(1 - \mathbf{n} \cdot \boldsymbol{\beta})^3} \Big|_{\text{ret.}} \quad (\text{A2})$$

We take the viewpoint of an observer at an angle  $\theta$  between the line of sight and the magnetic field lines. Assuming a large distance between the source and the observer we approximate the distance at the retarded time  $t = \tau + R(\tau)/c$  as

$$R(\tau) \approx R - \mathbf{n} \cdot \mathbf{r}(\tau) \quad (\text{A3})$$

The vector

$$\mathbf{r}(\tau) = \frac{\beta c}{\omega_s} \begin{pmatrix} \sin \alpha \cos \phi \\ \sin \alpha \cos \theta \sin \phi - \tau \omega_s \sin \theta \cos \alpha \\ \sin \alpha \sin \theta \sin \phi + \tau \omega_s \cos \theta \cos \alpha \end{pmatrix} \quad (\text{A4})$$

describes the path of the spiraling electron with the azimuth angle  $\phi = \omega_s \tau$  inside the source and  $\mathbf{n} = (0, 0, 1)$  the line of sight in a coordinate system with the observer in the  $z$ -direction. If we take  $\theta$  to be a constant for sufficiently long times, it follows that  $\mathbf{n} \cdot \mathbf{r}(\tau)$  becomes a periodic function in  $\tau$ . This forces us to expand the electric field as was previously stated by Shu (1991). Thus the spectrum of a single electron decomposes into discrete emission lines with Fourier coefficients given by

$$\mathbf{g}_m = \frac{\omega}{2\pi} \int_{-\frac{\pi}{\omega}}^{\frac{\pi}{\omega}} dt \mathbf{g}(t) \exp[-im\omega t] \quad (\text{A5})$$

and the time average of the observed power is provided by Parseval's theorem

$$P(\Omega) = \nu \int_0^{\frac{1}{\nu}} dt P(\Omega, t) = \frac{q^2}{2\pi c} \sum_{m=1}^{\infty} |\mathbf{g}_m| \quad (\text{A6})$$

and the symmetry of  $\mathbf{g}_m$  with respect to  $m \rightarrow -m$ . We trace back the integral to the retarded time and, following the derivation given by Bekefi (1966), we obtain

$$-im\omega t \approx -im(\omega_s \tau - \psi \sin(\omega_s \tau)) \quad (\text{A7})$$

for the argument of the exponential function. This provides us with a parameter reflecting the geometry,  $\psi$ , and connects the frequency of the spiral with the frequency measured by the observer  $\omega$ . The derivative of the light cone condition

$$dt = d\tau \left( 1 + \frac{dR(\tau)}{c d\tau} \right) \quad (\text{A8})$$

allows a substitution of the integration variable  $t$  by  $\tau$  in the same way as Jackson (1962 Cap. 14.5). Using approximation (A3) and the identity

$$\frac{d}{d\tau} \frac{\mathbf{n} \times [\mathbf{n} \times \boldsymbol{\beta}]}{1 - \mathbf{n} \cdot \boldsymbol{\beta}} = (1 - \mathbf{n} \cdot \boldsymbol{\beta}) \mathbf{g}(\tau) \quad (\text{A9})$$

we perform a partial integration of (A5) and get

$$\mathbf{g}_m = -\frac{im\omega^2}{2\pi} \int_{-\tau_1}^{\tau_1} d\tau \mathbf{g}_1 \exp[-im\omega t] \quad (\text{A10})$$

with

$$\mathbf{g}_1 = \begin{pmatrix} \sin \alpha \sin \phi \\ -\sin \alpha \cos \theta \cos \phi + \sin \theta \cos \alpha \\ 0 \end{pmatrix} \quad (\text{A11})$$

$$t = (\tau(1 - \beta \cos \alpha \cos \theta) - \beta \omega_s^{-1} \sin \alpha \sin \theta, \sin(\omega_s \tau))$$

The contribution from the boundary in the partial integration vanishes if the argument is periodic with period  $2\pi \omega^{-1}$  which determines the frequency  $\omega = (1 - \beta \cos \theta \cos \alpha)^{-1} \omega_s$  seen by the observer. Changing the variable of integration from  $\tau$  to  $\phi$  we get

$$\mathbf{g}_m = \frac{im\omega_s \beta}{2\pi \xi^2} \int_{-\pi}^{\pi} d\phi \mathbf{g}_1 \exp[-im(\phi - \psi \sin \phi)] \quad (\text{A12})$$

with  $\psi$  and  $\xi$  defined in (5). The argument of the exp-function in (A12) is antisymmetric in  $\phi \rightarrow -\phi$  and the  $x$ -component of  $\mathbf{g}_1$  is also antisymmetric. The  $x$ -component of  $\mathbf{g}_m$  is given by the symmetric part of the integrand as

$$\begin{aligned} & \beta \frac{m\omega_s}{2\pi \xi^2} \sin \alpha \int_0^{\pi} d\phi [\cos((m-1)\phi - m\psi \sin \phi) \\ & - \cos((m+1)\phi - m\psi \sin \phi)] \end{aligned} \quad (\text{A13})$$

Taking the integral representation for Bessel functions of integer order (e.g. Abramowitz & Stegun 1972 [9.1.21])

$$\pi J_m(z) = \int_0^\pi d\phi \cos(z \sin \phi - m\phi) \quad (\text{A14})$$

and the recurrence relation  $J_{m-1}(z) - J_{m+1}(z) = 2J'_m(z)$  the  $x$ -component of  $\mathbf{g}_m$  becomes

$$\frac{m\omega_s}{\xi^2} \beta \sin \alpha J'_m(m\psi) \quad (\text{A15})$$

The  $y$ -component of  $\mathbf{g}_1$  is symmetric and the part contributing to the  $y$ -component of  $\mathbf{g}_m$  is

$$i \frac{m\omega_s}{2\xi^2} \beta [2 \cos \alpha \sin \theta J_m(m\psi) - \sin \alpha \cos \theta (J_{m-1}(m\psi) + J_{m+1}(m\psi))] \quad (\text{A16})$$

With an additional recurrence relation  $J_{m-1}(z) + J_{m+1}(z) = 2mz^{-1}J_m(z)$  the  $y$ -component of  $\mathbf{g}_m$  can be rewritten as

$$i \frac{m\omega_s}{\xi^2} \frac{\beta \cos \alpha - \cos \theta}{\sin \theta} J_m(m\psi) \quad (\text{A17})$$

The two representations (A15) and (A17) for the two components of the electric field are presented in Eq. (4).

## Appendix B: The Volume-Integral of Received Power

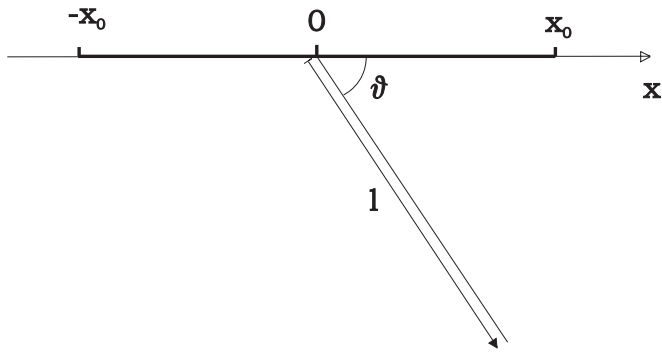


**Fig. B1.** Geometry of the the source region and choice of coordinates.

### B.1. Geometry and Coordinates

We consider the emission of synchrotron radiation by relativistically moving electrons in a homogeneous magnetic field which is inclined to the observer by an angle  $\vartheta$ . The source is located far from the observer and is unresolved, so that the received power does not depend on the position of the emitting electron inside the source. Due to the motion of an individual electron along the magnetic field with velocity  $v_{\parallel} = c\beta_{\parallel}$ , this electron is seen by the observer for a time  $\Delta t = v_{\parallel}x^{-1}(1 \pm |\beta_{\parallel}| \cos \vartheta)$  if  $x$  is the length of the electron's path along the magnetic field during the observation. The time interval is shortened for electrons approaching the

observer and prolonged for those which are receding. For calculating the observed power, Scheuer (1968) showed that the received power of an individual electron is reduced by a factor  $(1 \pm \beta_{\parallel} \cos \vartheta)$  since it contributes to the total power only for a velocity-dependent time interval. When dealing with a distribution function in phase space describing the electrons in the source we show here that this argument must be based on the invariance of the distribution function to get the same result. In order to simplify the discussion we consider the source to be a box of length  $2x_0$  with the magnetic field directed along the  $x$ -axis and the centre of the coordinate system centered in the box. Suppose we have two fluxes of electrons all of the same energy. One moving in the negative  $x$ -direction with velocity  $-v_{\parallel}$  and the other in the positive direction with  $v_{\parallel}$ . Synchrotron radiation should only be emitted while the electrons are inside the box and the distance between two neighbouring electrons moving in the same direction is  $x_0/N$ . The distribution of electrons can be written as

$$f(x) = \Theta(x_0 - |x|) \left[ \sum_n \delta \left( x - n \frac{x_0}{N} + c\beta_{\parallel} t \right) + \sum_m \delta \left( x + m \frac{x_0}{N} - c\beta_{\parallel} t \right) \right] \quad (\text{B1})$$

For each emitting electron it takes a time  $\Delta t_e$  for the radiation to arrive at the position of the observer, given by

$$\Delta t_e = c^{-1} (l - x \cos \vartheta) \quad , \quad (\text{B2})$$

which depends on the distance between source and observer  $l$  which is omitted in the following analysis.

### B.2. Normalizing the Distribution

In general the distribution function and its integral in phase space is an invariant due to changes in the variables. This can be expressed as

$$\int_{\Delta t} dt \int d^3r d^3p \hat{f}(\mathbf{r}, \mathbf{p}, t) = 4N\Delta t$$

with the knowledge of the energy equation  $E^2 = p^2 c^2 + m_e^2 c^4$ . We have  $4N$  electrons on average in the volume of interest and the complete distribution function of our problem reads

$$\hat{f} = [\delta^3(\mathbf{p} - \mathbf{p}_0) + \delta^3(\mathbf{p} + \mathbf{p}_0)] \Theta(x_0 - |x|) \delta(y - y_0) \delta(z - z_0) \sum_n \delta \left( x - n \frac{x_0}{N} - \frac{p_x}{m_e} t \right) \quad (\text{B3})$$

where we used the momentum  $\mathbf{p}_0 = (v_{\parallel} m_e, 0, 0)$ . Performing the simple integrals gives us

$$4N\Delta t = \int_{\Delta t} dt \int dx \int dp_x \tilde{f}(x, p_x, t) \quad .$$

If we want to express the integral in terms of the arrival time of signals at the observer  $\tilde{t} = t + \frac{x}{c} \cos \vartheta$ , we have to change the integration variables, resulting in a factor

$$\frac{\partial(\tilde{x}, \tilde{p}_x, \tilde{t})}{\partial(x, p_x, t)} = 1 + \frac{p_x}{m_e c} \cos \vartheta$$

with  $\tilde{x} = x$  and  $\tilde{p}_x = p_x$ . So, whenever we calculate mean values of observables  $P(x, p_x, t)$  in terms of  $x, \tilde{t}$ , we have to take

$$P(\tilde{t}) = \int_{-x_0}^{x_0} dx \left[ P_+ \sum_n \xi_+ \delta \left( x - n \frac{x_0}{N} + c\beta_{\parallel} \left( \tilde{t} + \frac{x}{c} \cos \vartheta \right) \right) + P_- \sum_m \xi_- \delta \left( x + m \frac{x_0}{N} - c\beta_{\parallel} \left( \tilde{t} + \frac{x}{c} \cos \vartheta \right) \right) \right] \quad (\text{B4})$$

$$\begin{aligned} \xi_+ &= 1 + \beta_{\parallel} \cos \vartheta & P_+ &= P(x, +p_0) \\ \xi_- &= 1 - \beta_{\parallel} \cos \vartheta & P_- &= P(x, -p_0) \end{aligned} \quad (\text{B5})$$

### B.3. Mean observed synchrotron power

If we know the received power for the two different types of electrons to be  $P_+, P_-$  we can integrate to get the total received power. If we collect terms containing  $x$  in the argument of the  $\delta$ -functions in (B4), we find

$$P(\tilde{t}) = \int_{-x_0}^{x_0} dx \left[ P_+ \xi_+ \sum_n \delta \left( \xi_+ x - n \frac{x_0}{N} + c\beta_{\parallel} \tilde{t} \right) + P_- \xi_- \sum_m \delta \left( \xi_- x + m \frac{x_0}{N} - c\beta_{\parallel} \tilde{t} \right) \right] \quad (\text{B6})$$

for the total power recieved. To evaluate the spatial integral we transform the argument of the  $\delta$ -functions

$$P = P_+ \int_{-x_0}^{x_0} dx \sum_n \delta \left( x - n \frac{x_0}{\xi_+ N} + c \frac{\beta_{\parallel} \tilde{t}}{\xi_+} \right) + P_- \int_{-x_0}^{x_0} dx \sum_m \delta \left( x + m \frac{x_0}{\xi_- N} - c \frac{\beta_{\parallel} \tilde{t}}{\xi_-} \right) \quad (\text{B7})$$

according to  $\int \delta(f(x)) dx = \sum_n \delta(x - x_n) \|f'(x_n)\|^{-1}$ . The conditions under which the electrons, which are counted by  $n$  and  $m$ , contribute to the integrals is

$$\begin{aligned} \left( \frac{c}{x_0} \beta_{\parallel} \tilde{t} - \xi_+ \right) N &\leq n < \left( \frac{c}{x_0} \beta_{\parallel} \tilde{t} + \xi_+ \right) N \\ \left( \frac{c}{x_0} \beta_{\parallel} \tilde{t} - \xi_- \right) N &\leq m < \left( \frac{c}{x_0} \beta_{\parallel} \tilde{t} + \xi_- \right) N \\ \Delta n &= 2\xi_+ N \quad \& \quad \Delta m = 2\xi_- N \end{aligned} \quad (\text{B8})$$

and we conclude that, for any instance of time, the number of electrons contributing to the integrals is  $2N\xi_+$  and  $2N\xi_-$  respectively. In this way the argument given above for the different time intervals is recovered. We see that the total received power is changed by this counting argument only because the change in the time as a variable  $t \rightarrow \tilde{t}$  is compensated by the invariance of the integral of the distribution function in  $\Gamma$ -space. This results in

$$P = 2N(1 + \beta_{\parallel} \cos \vartheta) P_+ + 2N(1 - \beta_{\parallel} \cos \vartheta) P_- \quad (\text{B9})$$

The results can alternatively be derived by multiplying the number of observed  $\delta$  electrons of each kind given in (B8) by the power recieved from these electrons. In this way, the result based on counting individual electrons (Scheuer 1968, Rybicky & Lightman 1979), can be recovered.

## References

- Abramowitz M., Stegun I.A. (eds.), 1972, Handbook of Mathematical Functions, Dover Publications, New York
- Beckert T., Duschl W.J., Mezger P.G., Zylka R., 1996, A&A 307, 450, [B96]
- Bekefi G., 1966, Radiation Processes in Plasmas, John Wiley and sons, New York
- Blumenthal G.R., Gould R.J., 1970, Rev. Mod. Phys 42, 237
- de Bruyn A. G., 1976, A&A 52, 439
- Duschl W.J., Lesch H., 1994, A&A 286, 431
- Ginzburg V.L., Sazomov V., Syrovatsky S.I., 1968, Usp. Fiz. Nauk 94, 63, [Sov. Phys. Usp. 11, 34]
- Ginzburg V.L., Syrovatsky S.I., 1969, ARA&A , 7, 375
- Eckart A., Genzel R., 1997, MNRAS 284, 576
- Epstein R.I., Feldman P.A., 1967, ApJ 150, L109
- Falcke H., Goss W.M., Ho L.C., 1997, IAU-Coll. 164, in press
- Jackson J.D., 1962, Classical Electrodynamics, John Wiley & Sons , New York
- Landau L.D., Lifschitz E.M., 1992, Klassische Feldtheorie, Akademie Verlag, Berlin
- Mahadevan R., Narayan R., Yi I., 1996, ApJ 465, 327
- Melia F., 1994, ApJ 426, 577
- Morrison R., McCammon D., 1983, ApJ 270, 119
- Narayan R., Yi I., Mahadevan R., 1995, Nature 374, 623
- Pavlinsky M. N., Grebenev S. A., Sunyaev R. A., 1994, ApJ 425, 110
- Predehl P., Trümper J., 1994, A&A 290, L29
- Reuter H.-P., Lesch H., 1996, A&A 310, L5
- Rybicky G. B., Lightman A. P., 1979, Radiative Processes in Astrophysics, John Wiley & Sons, New York
- Scheuer P.A.G., 1968, ApJ 151, L139
- Schlickeiser R., 1984, A&A 136, 227
- Schwinger J., 1949, Phys. Rev. 75, 1912
- Shu F. H., 1991, The Physics of Astrophysics (Vol.1), University Science Books, Mill Valley
- Watson M.G., Willingale R., Grindlay J.E., Hertz P., 1981, ApJ 250, 142
- Westfold K.C., 1959, ApJ 130, 241
- Wittkowski M., Balega Y., Beckert T., et al., 1997, A&A , submitted
- Zylka R., Mezger P.G., Ward-Thompson D., Duschl W.J., Lesch H., 1995, A&A 297, 83